

Entanglement Properties of Localized States in 1D Topological Quantum Walks

C.M. Chandrashekar,^{1,*} H. Obuse,^{2,†} and Th. Busch^{1,‡}

¹*Quantum Systems Unit, Okinawa Institute of Science and Technology Graduate University, Okinawa, Japan*

²*Department of Applied Physics, Hokkaido University, Sapporo 060-8628, Japan*

The symmetries associated with discrete-time quantum walks (DTQWs) and the flexibilities in controlling their dynamical parameters allow to create a large number of topological phases. An interface in position space, which separates two regions with different topological numbers, can, for example, be effectively modelled using different coin parameters for the walk on either side of the interface. Depending on the neighbouring numbers, this can lead to localized states in one-dimensional configurations and here we carry out a detailed study into the strength of such localized states. We show that it can be related to the amount of entanglement created by the walks, with minima appearing for strong localizations. This feature also persists in the presence of small amounts of σ_x (bit flip) noise.

I. INTRODUCTION

Quantum walks^{1,2} can be used to efficiently create non-classical states and have therefore been of large interest for designing quantum algorithms^{3–9} and realizing universal quantum computation^{10,11}. However, in recent years, quantum walks have also been employed to understand the dynamics of a considerable range of other physical processes, for example dielectric breakdown in driven electron system¹², transport in biological or chemical systems^{13–15} or effects in relativistic quantum dynamics^{2,16–19}. One of the more recent topics of interest is the creation of topological phases using quantum walks.

Topological properties of materials have recently been recognised as a rich source of interesting physics and have led to a new class known as topological insulators (TIs)^{20–22}. However, only a small number of natural TIs are known and therefore interest in creating artificial materials with non-trivial topological states is a prime research activity. Discrete-time quantum walks (DTQWs) are a method to create such states, as they can simulate time-independent lattice Hamiltonians with the required symmetries. At the same time they possess additional degrees of freedom, for example the possibility for varying coin operations, which can lead to much richer system^{23–28}. Progress in the theoretical understanding of these systems is going hand in hand with current advances in experimental implementations and engineering of quantum walks in various physical systems²⁹. Exploring topological phases using DTQWs has therefore emerged as a promising approach to realizing TIs in artificial materials.

The nontrivial topological phases of TIs are intricately linked to the presence or absence of certain symmetries, namely, time-reversal symmetry, particle-hole symmetry, and chiral symmetry³⁰. For one-dimensional DTQWs with the all three symmetries present (belonging to class BDI), the topological properties have recently been studied using a split-step²³ and a double split-step DTQW²⁷. Due to the 2π periodicity of the quasi-energies, the topological numbers of a 1D DTQW are defined not only for 0 but also for π quasi-energies, which means that they

become $\mathbb{Z} \times \mathbb{Z}$ winding numbers²⁷. Consequently, at the interface where two domains with different winding numbers are connected, topologically protected surface states appear at the two specific quasi-energies. Because of the one-dimensionality and the particle-hole symmetry, these surface states are the localized Majorana edge states, which have recently been experimentally observed²⁵.

As the winding number is a function of the angle θ_i used in the quantum coin operation for each split-step, the phase diagram of a TI can be written in terms of the angle on either side of the interface. This allows to identify the combinations that lead to the appearance of localized states at the interface, but does not give any information about the strength of the localization, i.e. the probability of finding the particle at the interface. While for some configurations the localization is very strong and only a small probability of finding the particle away from the interface exist, for other configurations it can be weaker. Knowing which configurations result in strongly topologically localized states is necessary to identify parameters that lead to TIs with a strongly insulating band-structure.

In the following we will show that strong localization at the interface due to topological effects can be signaled by a minimum in entanglement generated during split-step and double split-step DTQWs. This is in contrast to the properties found for localized states due to disordered coin operations in DTQWs, where for the standard DTQW an enhancement of entanglement is seen for temporal^{31,32} and spatio-temporal disorder and only a small decrease is seen for purely spatial disorder³¹. In addition, we will also discuss the effect of noise on topologically localized states and show that they are robust against σ_x (bit flip) noise.

II. TOPOLOGICAL QUANTUM WALKS

A 1D DTQW is defined for a system composed of a particle space and a position space. The basis states of the particle space can be any two internal states represented by $|0\rangle$ and $|1\rangle$ and the basis states of the

position space are defined on $|x\rangle$, where x is an integer. If the initial state is given by a particle in state $|\Psi_{\text{in}}\rangle = (\alpha|0\rangle + \beta|1\rangle) \otimes |x=0\rangle$, which is located at the origin, each step of the walk is composed of a quantum coin operation

$$R_\theta \equiv \begin{bmatrix} \cos(\theta/2) & -\sin(\theta/2) \\ \sin(\theta/2) & \cos(\theta/2) \end{bmatrix} \otimes \mathbb{I}, \quad (1)$$

followed by a position shift operation

$$S = |0\rangle\langle 0| \otimes |x-1\rangle\langle x| + |1\rangle\langle 1| \otimes |x+1\rangle\langle x|. \quad (2)$$

The unitary operator $W(\theta) = SR_\theta$ therefore defines one step of the standard DTQW and the state after t steps is given by $|\Psi_t\rangle = [SR_\theta]^t |\Psi_{\text{in}}\rangle$.

The eigenstates of the single time step operator can be written as

$$W(\theta)|\psi_\varepsilon\rangle = e^{-i\varepsilon}|\psi_\varepsilon\rangle, \quad (3)$$

where the quasi-energies ε are real and have 2π periodicity. These spectral properties of $W(\theta)$ give insight into the long time behavior of the walk and therefore also the behavior of topologically protected localized states.

Nontrivial topological phases in DTQW can be found when the evolution operator $W(\theta)$ indicates the presence of certain specific symmetries, such as time-reversal, particle-hole, or chiral symmetries. For 1D systems particle-hole or chiral symmetries are known to be important³⁰ to lead to two different topological numbers, ν_0 and ν_π , for the quasi-energies $\varepsilon = 0$ and π , which in turn leads to edge states that are localized at the interfaces across which the topological numbers change²⁷.

As all the matrix elements of the operator $W(\theta)$ used for defining the DTQW above are real, particle-hole symmetry is automatically guaranteed. To ensure chiral symmetry for $W(\theta)$ one needs to ensure the existence of a chiral operator Γ which satisfy the relation

$$\Gamma W(\theta) \Gamma^{-1} = W(\theta)^{-1}, \quad (4)$$

For this we will first decompose the operator $W(\theta)$ as

$$W(\theta) = F \cdot G, \quad (5)$$

where F and G are two sub-steps with each being a composition of coin (R_θ) and shift operator (S). They are related by

$$\Gamma F \Gamma^{-1} = G^{-1}, \quad (6)$$

and the above expression is guaranteed if the components of both, F and G , satisfy

$$\Gamma R_\theta \Gamma^{-1} = R_\theta^{-1} \quad \text{and} \quad \Gamma S \Gamma^{-1} = S^{-1}. \quad (7)$$

This leads to a chiral symmetry operator of the form

$$\Gamma \equiv \sigma_x \otimes \mathbb{I}, \quad \text{with} \quad \sigma_x = \begin{bmatrix} 0 & 1 \\ 1 & 0 \end{bmatrix}. \quad (8)$$

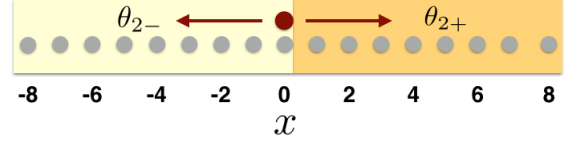


FIG. 1: Schematic of the position space showing the boundary created by θ_{2-} and θ_{2+} , which leads to the appearance of topological properties.

The topological numbers (ν_0, ν_π) of the 1D DTQW stemming from this kind of chiral symmetry have been calculated recently²⁷. If $W(\theta)$ satisfies chiral symmetry (Eq. (4)), a counterpart state with opposite sign of the quasi-energy is guaranteed,

$$W(\theta)|\psi_{-\varepsilon}\rangle = e^{+i\varepsilon}|\psi_{-\varepsilon}\rangle, \quad (9)$$

where

$$|\psi_{-\varepsilon}\rangle \equiv \Gamma|\psi_\varepsilon\rangle. \quad (10)$$

Taking into account the 2π periodicity of ε , the above relation for the edge states at $\varepsilon = 0$ and π is therefore identical to the eigenstate equation of the chiral symmetry operator Γ ,

$$\Gamma|\psi_{0,\pi}\rangle = \pm|\psi_{0,\pi}\rangle, \quad (11)$$

with the eigenvalues ± 1 .

In the following we will focus on two specific DTQW with chiral symmetry and discuss their topological properties. First we consider a DTQW with each step split into two with different coin parameters θ_i ²³ as

$$W(\theta_1, \theta_2) = S_+ R_{\theta_2} S_- R_{\theta_1}, \quad (12)$$

and for which the position split shift operators are

$$S_- = |0\rangle\langle 0| \otimes |x-1\rangle\langle x| + |1\rangle\langle 1| \otimes |x\rangle\langle x|; \quad (13)$$

$$S_+ = |0\rangle\langle 0| \otimes |x\rangle\langle x| + |1\rangle\langle 1| \otimes |x+1\rangle\langle x|. \quad (14)$$

To create a real space boundary between topologically distinct phases and reveal non-trivial topological properties at the interface, one can choose different θ_2 to the left ($R_{\theta_{2-}}$) and right side ($R_{\theta_{2+}}$) of a point in the position space as shown in Fig. 1, while defining the coin operation R_{θ_1} uniformly on the entire position space.

The topological numbers (ν_0, ν_π) for this split-step DTQW as a function of the coin parameters θ_1 and θ_2 are shown in Fig. 2²⁶. Using this phase diagram one can identify combinations of θ_{2-} and θ_{2+} that are located in regions with different topological numbers and therefore lead to an interface where a localized state can exist.

Examples of the behaviour can be seen in Figs. 3(b) and 3(d), where we show the spatial probability distribution after 100 steps for $(\theta_1, \theta_{2+}, \theta_{2-}) =$

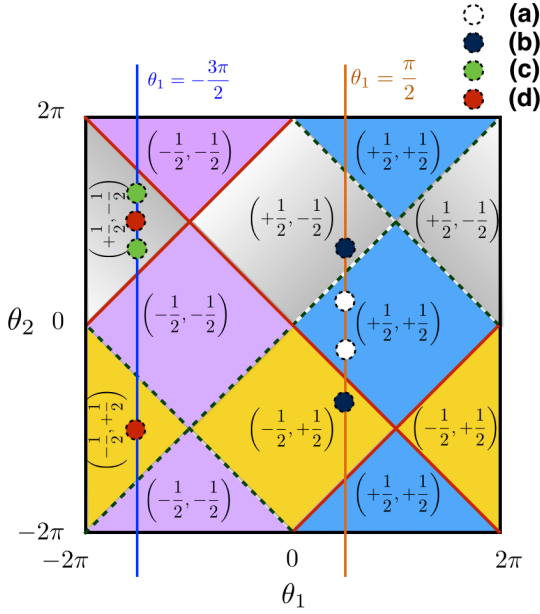


FIG. 2: Phase diagram of the topological numbers (ν_0, ν_π) associated with the split-step DTQW as a function of the coin parameters θ_1 and θ_2 . Topologically distinct gapped phases are separated by lines where the gap closes at either $\varepsilon = 0$ (solid lines) or $\varepsilon = \pi$ (dashed lines). Four pairs of circles with different colours and labeled as (a), (b), (c) and (d) are marked to identify different parameters corresponding to the probability distributions shown in Fig. 3.

$(\pi/2, -3\pi/4, 3\pi/4)$ and $(-3\pi/2, -\pi, \pi)$. In both cases localization is clearly visible. If, on the other hand, θ_{2+} and θ_{2-} correspond to regions with the same topological number, the probability at $x = 0$ decreases with time, indicating the absence of a localized state. Examples of this are shown in Figs. 3(a) and 3(c) for values of $(\theta_1, \theta_{2+}, \theta_{2-}) = (\pi/2, -\pi/4, \pi/4)$ and $(-3\pi/2, 5\pi/4, 3\pi/4)$, respectively.

A second class of DTQWs with rich topological features are double split-step evolutions²⁷. These are described by four parameters θ_i , leading to an effective Hamiltonian with long range hopping that results in higher values for winding numbers and topological numbers. Each step in the double split-step walk is a composition of the operators

$$W(\theta_1, \theta_2, \theta_3, \theta_4) = S_+ R_{\theta_4} S_+ R_{\theta_3} S_- R_{\theta_2} S_- R_{\theta_1}, \quad (15)$$

where setting $\theta_2 = \theta_4$ ensures chiral symmetry (CS). For simplicity we will also set $\theta_1 = 0$ in the following and in Fig. 4 we show the phase diagram as function of θ_2 and θ_3 . Regions with different topological numbers can again be clearly identified²⁷ and in Fig. 5 examples of spatial probability distributions for the situation in which different coin parameters have been used on the left and the right of the initial position, creating a boundary at the origin, are shown. The four pairs of parameters (θ_2, θ_3) used to generate

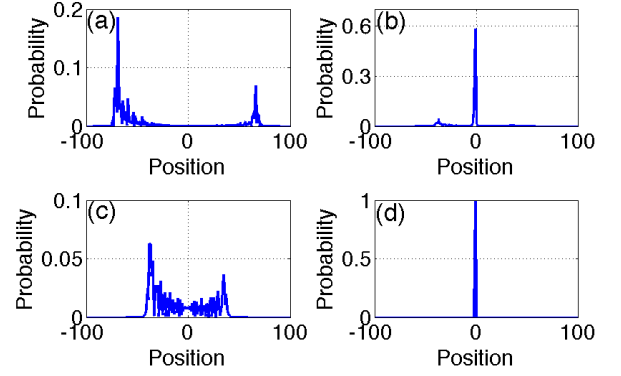


FIG. 3: Probability distributions of the split-step DTQW after 100 steps with a particle initially in the state $|\Psi_{\text{in}}\rangle = \frac{1}{\sqrt{2}}(|0\rangle + |1\rangle) \otimes |x = 0\rangle$. For (a) and (b) $\theta_1 = \pi/2$ and $(\theta_{2-}, \theta_{2+}) = (-\pi/4, \pi/4)$ and $(-3\pi/4, 3\pi/4)$, respectively. For (c) and (d) $\theta_1 = -3\pi/2$ the $(\theta_{2-}, \theta_{2+}) = (5\pi/4, 3\pi/4)$ and $(-\pi, \pi)$, respectively. These parameters correspond to the circles in Fig. 2 and are chosen such that in (a) and (c) the θ_{2-} and θ_{2+} are from regions with the same topological invariant, whereas in (b) and (d) they stem from regions with distinct topological numbers.

these probability distributions are marked with circles of different color in the phase diagram (Fig. 4). For the parameters $(\theta_{2-}, \theta_{2+}; \theta_{3-}, \theta_{3+}) = (-\pi/8, \pi/8; -\pi, \pi)$ and $(-3\pi/8, \pi/8; -3\pi/2, -\pi/2)$, chosen from regions with different topological numbers, the probabilities of finding the particle at $x = 0$ remains high, indicating the presence of localized state (see Figs. 5(b) and 5(d)). For the parameters $(\theta_{2-}, \theta_{2+}; \theta_{3-}, \theta_{3+}) = (-\pi/4, \pi/4; \pi, \pi)$ and $(-\pi/4, 3\pi/4; \pi/4, \pi/4)$, chosen from regions with same topological numbers, the probability of finding the particle at $x = 0$ is very low, indicating the dominance of diffusion (see Figs. 5(a) and 5(c)). One should note that it is possible to generate localized states for certain sets of parameters from the regions with the same topological invariant. Those, however, have energies different from 0 or π and are therefore distinguishable from localized states originating from topological effects.

III. ENTANGLEMENT PROPERTIES

DTQW are known to entangle the particle and the position space. The degree of entanglement depends on the parameters that define the evolution operators^{33,34} and it is intriguing to explore this quantity for topological quantum walks. While in the previous section localized states were shown to appear when choosing coin parameters for the left and right regions from areas with different topological numbers in the phase diagram, no indication could be drawn from this about the strength of the localized state. As often the probability of the diffusing component can be higher than the one of the localized part, it is important to identify the parameters that lead

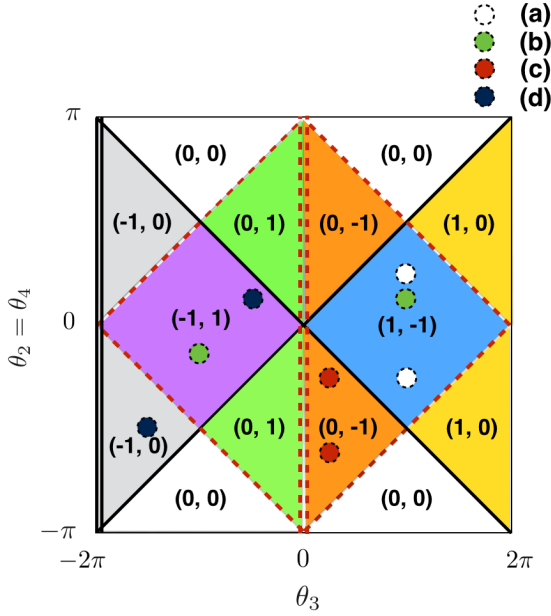


FIG. 4: Phase diagram of the topological numbers associated with double split-step DTQW as a function of the coin parameters θ_2 and θ_3 . The parameters θ_2 and θ_4 are set equal to ensure CS and we have chosen $\theta_1 = 0$. Topologically distinct gapped phases are separated by lines where the gap closes at either $\varepsilon = 0$ (solid lines) or $\varepsilon = \pi$ (dashed lines). Four pairs of circles with different shades labeled as (a), (b), (c) and (d) are marked to identify the different parameters used to generate probability distributions shown in Fig. 5.

to the highest probability for finding a strongly topologically localized state at $x = 0$, in order to create artificially synthesized TIs. In this section we ask and answer the question if entanglement is an effective measure to identify the configurations of parameters that result in strongly localized states. For this we calculate the entanglement generated by different topological quantum walks and identify the regions which lead to strongly localized states.

To quantify the entanglement between the particle and the position space we will use negativity, which is the absolute sum of the negative eigenvalues of the partial transpose of the density operator, $\rho = |\Psi_t\rangle\langle\Psi_t|$. It is given by

$$\mathcal{N}(\rho) = \sum_i \frac{|\lambda_i| - \lambda_i}{2} \quad (16)$$

where the λ_i are the eigenvalues of ρ .

To reduce the number of free parameters we initially fix $\theta_1 = -3\pi/2$ for the split-step DTQW and show in Fig. 6 the negativity as function of θ_{2-} and θ_{2+} . A varied landscape is clearly visible and to interpret the structure, one can map the diagram to the one for the topological numbers.

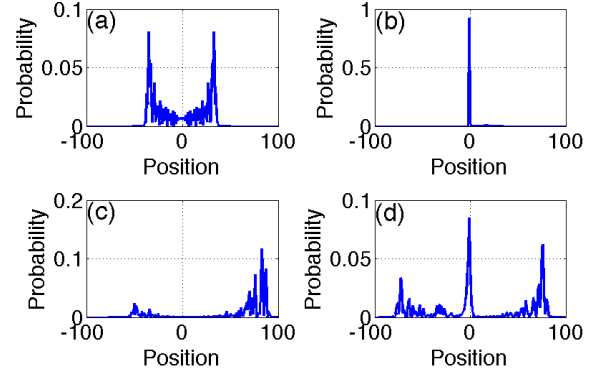


FIG. 5: Probability distributions of the double split-step DTQW after 50 steps of the walk for a particle with the initial state $|\Psi_{\text{in}}\rangle = \frac{1}{\sqrt{2}}(|0\rangle + |1\rangle) \otimes |x=0\rangle$. The chosen parameters for $(\theta_{2-}, \theta_{2+}; \theta_{3-}, \theta_{3+})$ are marked with circles in Fig. 4, (a) $(-\pi/4, \pi/4; \pi, \pi)$ (b) $(-\pi/8, \pi/8; -\pi, \pi)$, (c) $(-\pi/4, -3\pi/4; \pi/4, \pi/4)$ and (d) $(-3\pi/8, \pi/8; -3\pi/2, -\pi/2)$. The parameters in (a) and (c) are from regions with the same topological number and the absence of a localized state is evident, whereas the parameters in (b) and (d) are from regions with different topological numbers, which leads to localization.

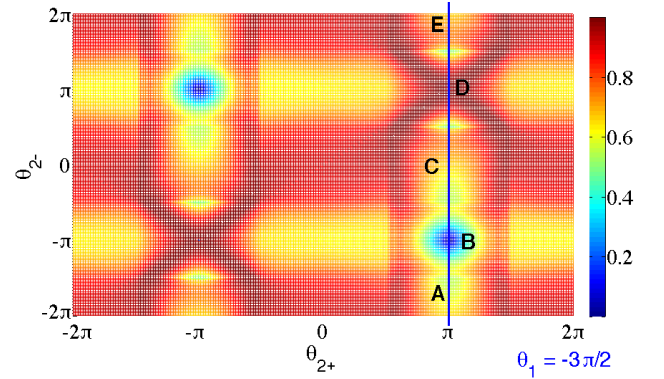


FIG. 6: Negativity as a function of θ_{2-} and θ_{2+} for the split-step DTQW with $\theta_1 = -3\pi/2$. The initial state was given by $|\Psi_{\text{in}}\rangle = \frac{1}{\sqrt{2}}(|0\rangle + |1\rangle) \otimes |x=0\rangle$ and the results are shown after 100 steps of walk.

For this we show in Fig. 7 the phase diagram again and the vertical line at $\theta_1 = -3\pi/2$ indicates the parameters for which the negativity is displayed in Fig. 6. If $\theta_{2+} = \pi$ (marked with a filled circle in region D) and θ_{2-} is ranging from -2π to 2π , one can see that the values of negativity have two clear trends. They are high if θ_{2-} is in a region with the same topological invariant as θ_{2+} (here the gray area around D) and low if θ_{2-} is in a region that has a different topological invariant. In fact, one can see that a minimum appears when θ_{2-} is from region B and we find that in general lower values of negativity indicate the presence of localized states with

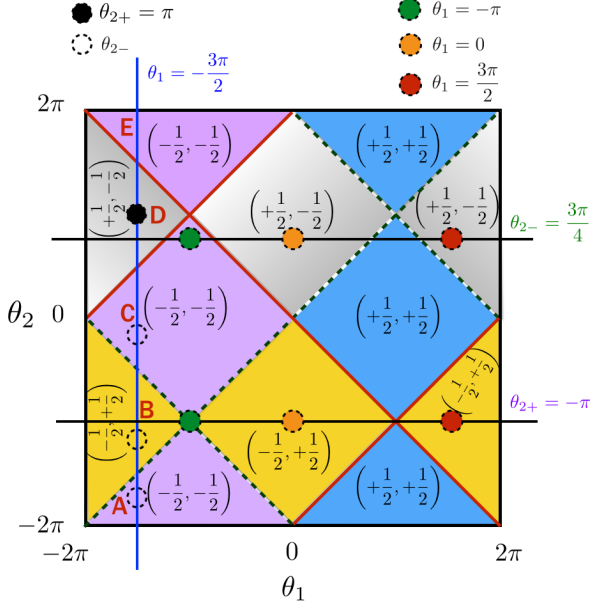


FIG. 7: Phase diagram of the split-step DTQW. The vertical line corresponds to the results shown in Fig. 6 and the horizontal lines corresponds to the negativity presented in Fig. 8.

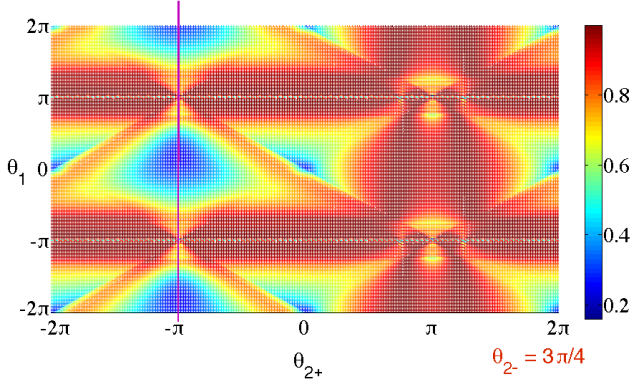


FIG. 8: Negativity of the split-step DTQW as a function of θ_1 and θ_{2+} for $\theta_{2-} = 3\pi/4$. The initial state was $|\Psi_{\text{in}}\rangle = \frac{1}{\sqrt{2}}(|0\rangle + |1\rangle) \otimes |x=0\rangle$ and the results shown are after 100 steps of walk.

smaller fractions of the particle's amplitude diffused. (see Fig. 3(d)).

In Fig. 8 we show the negativity as a function of θ_1 and θ_{2+} by fixing $\theta_{2-} = 3\pi/4$. When $\theta_{2+} = -\pi$ the values of θ_{2-} and θ_{2+} will be in regions with different topological numbers for all values of θ_1 , except for $\theta_1 = \pm\pi$, where regions of different topological numbers meet. This can be seen from Fig. 7 where the two horizontal lines indicate the topological regions in which θ_{2-} and θ_{2+} lie when θ_1 is ranging from -2π to 2π . The correspond-

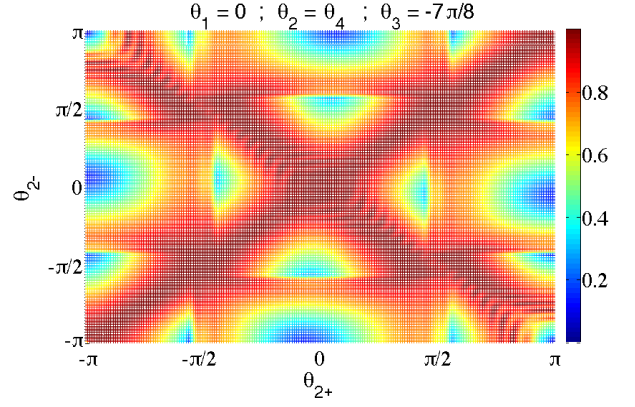


FIG. 9: Negativity of the double split-step DTQW as a function of θ_{2-} and θ_{2+} when $\theta_1 = 0$, $\theta_3 = -7\pi/8$ and $\theta_{4\pm} = \theta_{2\pm}$. The initial state was $|\Psi_{\text{in}}\rangle = \frac{1}{\sqrt{2}}(|0\rangle + |1\rangle) \otimes |x=0\rangle$ and the results shown are after 50 steps of walk.

ing values of negativity correspond to the vertical line in Fig. 8 and one can clearly see low values of negativity for all values of θ_1 , except at the points $\theta_1 = \pm\pi$. A general comparison of the phase diagram (Fig. 7) and the negativity profiles (Figs. 6 and 8) for different combinations of θ_1 , θ_{2-} and θ_{2+} shows that low values for the negativity appear whenever the combination of θ_{2-} and θ_{2+} is chosen from regions with different topological invariant. This indicates that a low area in the negativity landscape can be effectively used to identify the combinations that result in localized states, with the minima corresponding to localized states with zero or minimal diffusion component.

Similarly, a negativity plot for the double split-step DTQW can be effectively used to identify the combination of parameters which lead to strongly localized states. In Fig. 9 we show the negativity as a function of θ_{2+} and θ_{2-} for $\theta_1 = 0$, $\theta_3 = -7\pi/8$ and $\theta_{4\pm} = \theta_{2\pm}$. The visible valleys of entanglement corresponds to parameter ranges in which a strongly localized state is obtained.

This observation is in contrast to the behavior of entanglement for localization in 1D DTQW using disordered quantum coin operations. With spatially disordered coin operations, only a small decrease in entanglement is seen when compared to the entanglement due to standard DTQW³¹ and with temporally and spatio-temporally disordered coin operations, enhancement of entanglement is seen^{31,32}. Though the states are localized, the degree of entanglement is not significantly affected because of the longer localization length of the disordered localized state when compared to the short localization length of topologically localized states.

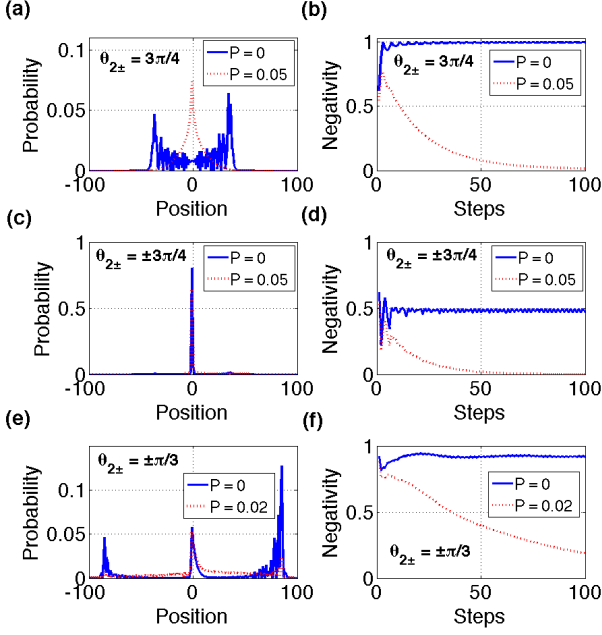


FIG. 10: Effect of σ_x noise on the split-step DTQW for different configurations of $\theta_{2\pm}$ when $\theta_1 = -\pi/4$. (a), (c) and (e) show the probability distribution after 100 steps of walk in the absence and in the presence of noise. (b), (d) and (f) show the negativity as a function of the number of steps in absence and in presence of noise. The probability distributions show that the noise affects the diffusing part of the walk significantly but hardly influences the topologically localized part.

IV. STRENGTH OF THE LOCALIZED STATE IN THE PRESENCE OF NOISE

The application of noise to DTQWs is known to result in decoherence^{33,35}, however small amounts of noise can also be advantageous for quantum algorithms and quantum transport. Here we will look into the effect of $\sigma_x = \begin{bmatrix} 0 & 1 \\ 1 & 0 \end{bmatrix}$ (bit flip) noise on the topological quantum walk and show its effect on the localized and diffusive components.

The operation used for describing the two split-step DTQW evolution with σ_x noise is given by

$$\rho(t) = P[f_1 W(\theta_1, \theta_2) \rho(t-1) W(\theta_1, \theta_2)^\dagger f_1^\dagger] + (1-P) W(\theta_1, \theta_2) \rho(t-1) W(\theta_1, \theta_2)^\dagger, \quad (17)$$

where $\rho(0) = |\Psi_{\text{in}}\rangle\langle\Psi_{\text{in}}|$, $W(\theta_1, \theta_2)$ is same as Eq. (12), $f_1 \equiv \sigma_x \otimes \mathbb{I}$ and P is the magnitude of noise. No noise is described by $P = 0$ and due to the fact that symmetries are not effected by bit flip noise, the maximum noise corresponds to $P = 0.5$ ³⁵.

In Fig. 10 we show the probability distributions and the corresponding values of negativity for the split-step

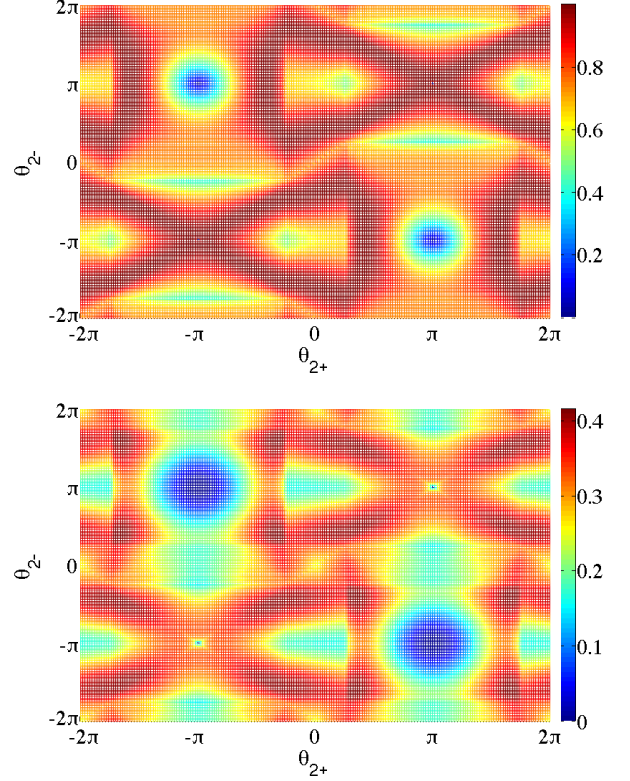


FIG. 11: Negativity as a function of θ_{2-} and θ_{2+} for $\theta_1 = -\pi/4$ for the noiseless ($P = 0.00$, upper) and the noisy ($P = 0.02$, lower) split-step DTQW. Note the difference in the color scale.

DTQW for different configurations of $\theta_{2\pm}$ in the presence and absence of noise. Applying noise to an evolution which in the absence of noise leads to a delocalized state (see Fig. 10(a), blue line), now leads to a state that is located around the origin. For a combination of $\theta_{2\pm}$ parameters resulting in a probability distribution with both, localized and a diffusive components (see Fig. 10(c) and (e)) the effect of noise results in a reduction of the probability for spreading in position space away from the origin, while the effect on the localized part is very small. This indicates a robustness of topologically localized states to noise, which is absent for diffusive states. This behaviour is also reflected in the negativity and in Figs. 10(b) and (d) and can see that the non-zero value of negativity in the absence of noise, indicative of a diffusive component in the probability distribution, decreases fast when noise is present. Even for noise levels as small as $P = 0.02$, the effect of noise on the delocalized probability distribution is very strong, see Fig. 10(e).

In Fig. 11 we show the negativity as function of θ_{2-} and θ_{2+} when $\theta_1 = -\pi/4$ for evolutions without and with σ_x noise. One can see that the effect of the noise results in a decrease of the overall negativity, but remains essentially unchanged in the regions where strongly localized states appear. This indicates the robustness of the topologically

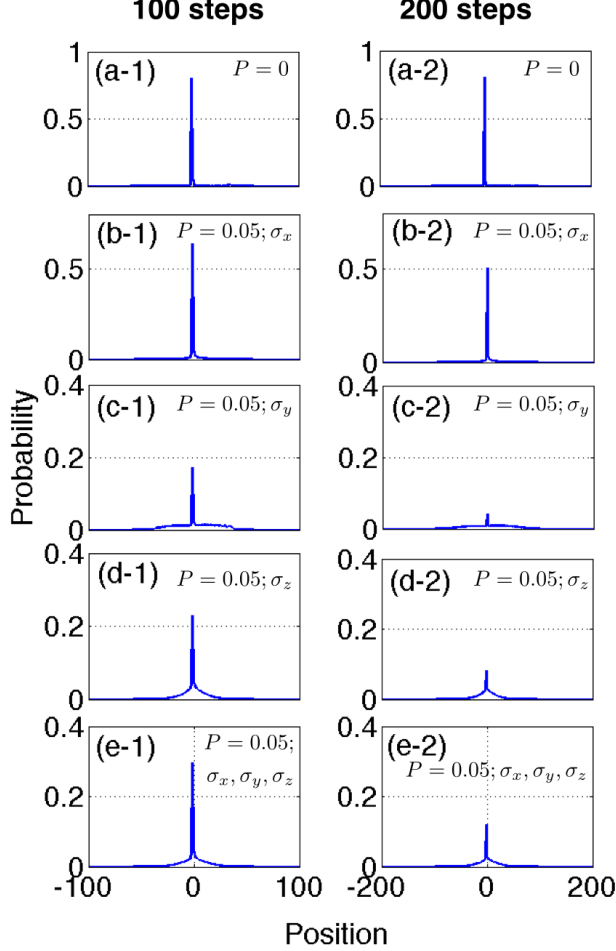


FIG. 12: Effect of noise on topologically localized states of the split step DTQW with $\theta_1 = -\pi/4$, $\theta_{2-} = -3\pi/4$ and $\theta_{2+} = 3\pi/4$. The first and second column show the probability distribution after 100 step and 200 step of evolution, respectively. The first row is the probability distribution for evolution without noise ((a-1), (a-2)), the second row is for evolution with σ_x noise ((b-1), (b-2)), the third row is for evolution with σ_y noise ((c-1), (c-2)), the fourth row is for evolution with σ_z noise ((d-1), (d-2)) and the fifth row is for evolution with depolarizing noise ((e-1), (e-2)). For all noisy evolutions the noise level is $P = 0.05$ and one can clearly see that the localized state is robust against σ_x but not other forms of noise, for which the localized component decays with increasing number of steps.

localized state against σ_x noise.

However, topologically localized states in the split-step DTQW are not robust to other forms of noise. In Fig. 12 we show the probability distributions for an evolution without (first row) and with noise (rest of the rows) after 100 (first column) and 200 (second column) steps. The σ_x noise is the same as given in Eq. (17) and the $\sigma_y = \begin{bmatrix} 0 & -i \\ i & 0 \end{bmatrix}$ and $\sigma_z = \begin{bmatrix} 1 & 0 \\ 0 & -1 \end{bmatrix}$ noises are obtained by

replacing σ_x by σ_y and σ_z in the Eq. (17). The operation to describe depolarizing noise is given by

$$\begin{aligned} \rho(t) = \frac{1}{3} & \left[f_1 W(\theta_1, \theta_2) \rho(t-1) W(\theta_1, \theta_2)^\dagger f_1^\dagger \right. \\ & + f_2 W(\theta_1, \theta_2) \rho(t-1) W(\theta_1, \theta_2)^\dagger f_2^\dagger \\ & + f_3 W(\theta_1, \theta_2) \rho(t-1) W(\theta_1, \theta_2)^\dagger f_3^\dagger \left. \right] \\ & + (1-P) W(\theta_1, \theta_2) \rho(t-1) W(\theta_1, \theta_2)^\dagger. \end{aligned} \quad (18)$$

Comparing the probability distributions of the localized states after evolution in the presence of these different kind of noises, one can clearly see that the topological states are robust only against σ_x noise and a significant decrease in localized probability at the interface is visible for all other forms of noise. From Eqs. (8) and (11) we can see that the edge states at $\varepsilon = 0$ and π are the eigenstates of the chiral symmetry operator Γ , which is identical to f_1 noise operator. Therefore this symmetry is preserved in the presence of f_1 noise and the edge state protected. However, this is not true for other forms of noise and the localized state can decay.

V. CONCLUSION

Engineering DTQWs with different combination of variable quantum coin and position shift operations allows to create a wide range of rich, topological phases. Choosing parameters θ_i with different topological numbers to the left and right side of an interface of the position space, leads to topology induced localized states, which are sometimes accompanied by a diffusing component. Identifying combinations resulting strong localization with minimal or completely absent diffusing components is important for simulations of artificial TIs and in this work we have shown that the negativity of a state can be used for such an identification. By exploring the negativity landscape as function of the quantum coin parameters we have linked the strength of the topologically localized states to the appearance of low values of the negativity.

These topology induced localized states are different from the localized states originating from disordered DTQWs, where the presence of entanglement is usually robust against disorder. This therefore allows to differentiate between topologically localized states and localized state due to spatial and dynamic disorder in 1D DTQW. Finally, we have demonstrated that the topologically localized component of a state is robust against σ_x noise, whereas the diffusing component decays. We strongly believe that studies like this can lead to better engineering of the artificial materials to realize TIs.

Acknowledgments

This work was supported by the Okinawa Institute of Science and Technology Graduate University. H.

O. was supported by Grant-in-Aid (Nos. 25800213 and 25390113) from the Japan Society for Promotion of Sci-

ence.

-
- * Electronic address: c.madaiah@oist.jp
† Electronic address: hideaki.obuse@eng.hokudai.ac.jp
‡ Electronic address: thomas.busch@oist.jp
- ¹ G. V. Riazanov, Sov. Phys., *The Feynman path integral for the Dirac equation*, Sov. Phys. JETP **6** 1107-1113 (1958); R. Feynman, *Found. Phys.* **16**, 507-531 (1986); K. R. Parthasarathy, *Journal of Applied Probability*, **25**, 151-166 (1988).
 - ² D. A. Meyer, *From quantum cellular automata to quantum lattice gases*, *J. Stat. Phys.* **85**, 551 (1996).
 - ³ A. Ambainis, *Int. J. Quantum. Inform.* **01**, 507 (2003).
 - ⁴ A. M. Childs, R. Cleve, E. Deotto, E. Farhi, S. Gutmann, and D. A. Spielman, *Exponential algorithmic speedup by quantum walk*, Proc. 35th ACM Symposium on Theory of Computing, pages 59-68 (2003).
 - ⁵ M. Szegedy, *Quantum speed-up of Markov chain based algorithms*, Foundations of Computer Science, 2004. Proceedings. 45th Annual IEEE Symposium on, pages 32-41 (2004).
 - ⁶ S. Aaronson and A. Ambainis, *Quantum search of spatial regions*, Theory of Computing, 1(4):47-79 (2005).
 - ⁷ F. Magniez and A. Nayak, *Quantum complexity of testing group commutativity*, Algorithmica, 48(3):221-232 (2007).
 - ⁸ A. Ambainis, *Quantum walk algorithm for element distinctness*, SIAM Journal on Computing, 37(1):210-239 (2007).
 - ⁹ F. Magniez, A. Nayak, P. Richter, and M. Santha, *On the hitting times of quantum versus random walks*, Algorithmica, 63(1):91-116 (2012).
 - ¹⁰ A.M. Childs, *Universal computation by quantum walk*, *Phys. Rev. Lett.* **102**, 180501 (2009).
 - ¹¹ N. B. Lovett, S. Cooper, M. Everitt, M. Trevers, and V. Kendon, *Universal quantum computation using the discrete-time quantum walk*, *Phys. Rev. A* **81**, 042330 (2010).
 - ¹² T. Oka, N. Konno, R. Arita, and H. Aoki, *Breakdown of an Electric-Field Driven System: A Mapping to a Quantum Walk*, *Phys. Rev. Lett.* **94**, 100602 (2005).
 - ¹³ Engel, G. S. et al., *Evidence for wavelike energy transfer through quantum coherence in photosynthetic systems*, *Nature* **446**, 782-786 (2007).
 - ¹⁴ Mohseni, M., Rebentrost, P., Lloyd, S. & Aspuru-Guzik, A. *Environment-assisted quantum walks in photosynthetic energy transfer*, *J. Chem. Phys.* **129**, 174106 (2008).
 - ¹⁵ Plenio, M. B. & Huelga, S. F. *Dephasing-assisted transport: quantum networks and biomolecules*, *New J. Phys.* **10**, 113019 (2008).
 - ¹⁶ F. D. Strauch, *Relativistic effects and rigorous limits for discrete- and continuous-time quantum walks*, *J. Math. Phys.* **48**, 082102 (2007).
 - ¹⁷ C. M. Chandrashekar, S. Banerjee, & R. Srikanth, *Relationship between quantum walks and relativistic quantum mechanics*, *Phys. Rev. A* **81**, 062340 (2010).
 - ¹⁸ Giuseppe, D. M., Debbasch, F. & Brachet, M. E., *Quantum walks as massless Dirac Fermion in curved space-time*, *Phys. Rev. A* **88**, 042301 (2013).
 - ¹⁹ C. M. Chandrashekar, *Two-component Dirac-like Hamiltonian for generating quantum walk on one-, two- and three-dimensional lattices*, *Scientific Reports* **3**, 2829 (2013).
 - ²⁰ M. Z. Hasan and C. L. Kane, *Colloquium: Topological insulators*, *Rev. Mod. Phys.* **82**, 3045 (2010).
 - ²¹ X.-L. Qi and S.-C. Zhang, *Topological insulators and superconductors*, *Rev. Mod. Phys.* **83**, 1057 (2011).
 - ²² J. E. Moore, *The birth of topological insulators*, *Nature (London)* **464**, 194-1998 (2010).
 - ²³ T. Kitagawa, M. S. Rudner, E. Berg, and E. Demler, *Exploring topological phases with quantum walks*, *Phys. Rev. A* **82**, 033429 (2010).
 - ²⁴ H. Obuse and N. Kawakami, *Topological phases and delocalization of quantum walks in random environments*, *Phys. Rev. B* **84**, 195139 (2011).
 - ²⁵ T. Kitagawa, M. A. Broome, A. Fedrizzi, M. S. Rudner, E. Berg, I. Kassal, A. Aspuru-Guzik, E. Demler, and A. G. White, *Observation of topologically protected bound states in photonic quantum walks*, *Nature Communications* **3**, 882 (2012).
 - ²⁶ J. K. Asbóth, *Symmetries, topological phases, and bound states in the one-dimensional quantum walk*, *Phys. Rev. B* **86**, 195414 (2012).
 - ²⁷ J. K. Asbóth and H. Obuse, *Bulk-boundary correspondence for chiral symmetric quantum walks*, *Phys. Rev. B* **88**, 121406(R) (2013).
 - ²⁸ B. Tarasinski, J. K. Asbóth, and J. P. Dahlhaus, *Scattering theory of topological phases in discrete-time quantum walks*, *Phys. Rev. A* **89**, 042327 (2014).
 - ²⁹ J. Du et al., *Phys. Rev. A* **67**, 042316 (2003); C. A. Ryan et al., *Phys. Rev. A* **72**, 062317 (2005); B. Do et al., *J. Opt. Soc. Am. B* **22**, 499 (2005); H. B. Perets et al., *Phys. Rev. Lett.* **100**, 170506 (2008); H. Schmitz et al., *Phys. Rev. Lett.* **103**, 090504 (2009); F. Zähringer et al., *Phys. Rev. Lett.* **104**, 100503 (2010); K. Karski et al., *Science* **325**, 174 (2009); A. Schreiber et al., *Phys. Rev. Lett.* **104**, 050502 (2010); M. A. Broome et al., *Phys. Rev. Lett.* **104**, 153602 (2010); A. Peruzzo et al., *Science* **329**, 1500 (2010); L. Sansoni et al., *Phys. Rev. Lett.* **108**, 010502 (2012); A. Schreiber K. N. Cassemiro, V. Potocek, A. Gábris, I. Jex, and Ch. Silberhorn, *Phys. Rev. Lett.* **106**, 180403 (2011); A. Crespi et al., *Nat. Phot.* **7**, 323 (2013); J. D. A. Meinecke et al., *Phys. Rev. A* **88**, 012308 (2013).
 - ³⁰ A. P. Schnyder, S. Ryu, A. Furusaki, and A. W. W. Ludwig, *Classification of topological insulators and superconductors in three spatial dimensions*, *Phys. Rev. B*, **78**, 195125 (2008).
 - ³¹ C. M. Chandrashekar, arXiv:1212.5984 (2012).
 - ³² R. Vieira, E. P. M. Amorim, and G. Rigolin, *Phys. Rev. Lett.* **111**, 180503 (2013).
 - ³³ O. Maloyer and V. Kendon, *Decoherence versus entanglement in coined quantum walks*, *New J. Phys.* **9**, 87 (2007).
 - ³⁴ S. K. Goyal and C. M. Chandrashekar, *Spatial entanglement using a quantum walk on a many-body system*, *J. Phys. A: Math. Theor.* **43**, 235303 (2010).
 - ³⁵ C. M. Chandrashekar, R. Srikanth, and S. Banerjee, *Symmetries and noise in quantum walk*, *Phys. Rev. A*, **76**, 022316 (2007).